An atomistic study of Y segregation at a $\{10\bar{1}1\}$–$\{10\bar{1}2\}$ double twin in Mg

Naoki Miyazawa, Shunya Suzuki, Mamoru Mabuchi, and Yasumasa Chino

COLLECTIONS

Paper published as part of the special topic on Chemical Physics, Energy, Fluids and Plasmas, Materials Science and Mathematical Physics

View Online

Export Citation

CrossMark

ARTICLES YOU MAY BE INTERESTED IN

An atomistic study of Y segregation at a {10$\bar{1}$1}–{10$\bar{1}$2} double twin in Mg

Naoki Miyazawa,[1,a] Shunya Suzuki,[1] Mamoru Mabuchi,[1]
and Yasumasa Chino[2]

[1]*Graduate School of Energy Science, Kyoto University, Yoshidahonmachi, Sakyo, Kyoto 606-8501, Japan*
[2]*Materials Research Institute for Sustainable Development, National Institute of Advanced Industrial Science and Technology, 2266-98 Anagahora, Shimo-shidami, Moriyama, Nagoya 463-8560, Japan*

Segregation at a triple junction of grain boundaries has not been explained much because the structure of a triple junction is very complicated. The present paper describes Monte Carlo simulations by which Y segregation was investigated at a triple junction of a {10$\bar{1}$1}–{10$\bar{1}$2} double twin in Mg. Y atoms segregated at the extension sites in the {10$\bar{1}$1} and {10$\bar{1}$2} twin boundaries. However, they were not necessarily more segregated at the triple junction of the double twin, although the free volumes at the extension sites of the triple junction were larger on average than those of the other boundaries. Thus, the Y segregation behavior at the triple junction cannot be explained only by the free volume. The anisotropic factor of the atomic Voronoi polyhedron was developed to explain the Y segregation behavior at the triple junction. In addition, the shortest interatomic distance and coordination number affected Y segregation at the triple junction. Also, segregation at the triple junction strongly depended on the Y concentration, which resulted from variations in the local atomic configuration. Thus, the Y segregation behavior at the triple junction was complicated, in contrast to those at twin boundaries, even when the size effect was predominant. © 2017 Author(s). All article content, except where otherwise noted, is licensed under a Creative Commons Attribution (CC BY) license (*http://creativecommons.org/licenses/by/4.0/*). [http://dx.doi.org/10.1063/1.4978534]

I. INTRODUCTION

Grain boundary segregation strongly affects material properties of polycrystallines. However, segregation at a triple junction (TJ) of grain boundaries has not been investigated much because the structure of a TJ is very complicated. Coincidence boundaries are convenient for investigating grain boundary segregation behavior from the atomistic view because atomic positions are known for many coincidence boundaries. So far there are many atomistic studies on grain boundary segregation at coincidence boundaries.[1–3] Thus, a TJ of coincidence boundaries is suggested to be suitable for investigating segregation at a TJ from the atomistic view.

Magnesium alloys are attracting much attention as structural light materials because they can reduce the environmental load by improving the fuel efficiency of vehicles, airplanes, and so on. Mg has few activated slip systems at room temperature because of its anisotropic hexagonal close-packed structure, and twinning is enhanced during deformation in Mg.[4,5] There are some deformation twinning modes in Mg.[6–11] In particular, {10$\bar{1}$1}<10$\bar{1}$2> and {10$\bar{1}$2}<10$\bar{1}$1> twinning significantly affect the mechanical properties of Mg.[10–15] It has been found that the {10$\bar{1}$1}–{10$\bar{1}$2} double twin (DT), which is composed of secondary {10$\bar{1}$2} twins in a primary {10$\bar{1}$1} twin, is formed at a final stage of deformation and provides a fracture-initiation site.[11,16–22] There are four possible variants

---

[a]Corresponding author. E-mail: miyazawa.naoki.37c@st.kyoto-u.ac.jp

(types 1–4) of double twinning in the DT, and the type 1 variant, which is the 38° <1$\bar{2}$10> variant, occurs most frequently.[23,24] Beyerlein *et al.*[25] proposed the formation mechanism of the DT through nucleation of the secondary twin in the primary twin domain. Recently, an atomistic simulation of the interaction of dislocations with the DT suggested that twinning dislocations, which are generated by absorption of dislocations into a {10$\bar{1}$1} twin boundary (TB),[14,26] pile up at the TJ of the DT, which induces cracking at the TJ.[26] It has been experimentally shown that addition of Y significantly improves the ductility of Mg.[26–29] Y tends to segregate at (twin) grain boundaries in Mg.[30,31] Hence, the enhanced ductility of Mg by Y addition may be related to Y segregation at DTs. However, there is little understanding of segregation at the DT.

TBs are typical of coincidence boundaries, and it is worthwhile to investigate segregation at the DT because there are TJs of TBs in the DT. In the present work, we performed Monte Carlo (MC) simulations of Y segregation at the DT, which is composed of a {10$\bar{1}$1} TB, a {10$\bar{1}$2} TB, a {30$\bar{3}$4} boundary, and a TJ, and the Y segregation behavior at the TJ was compared with those at the {10$\bar{1}$1} and {10$\bar{1}$2} TBs. Somekawa *et al.*[27] showed that certain Y addition was required to enhance the ductility of Mg. This suggests that Y segregation at the DT may depend on the Y concentration. Hence, MC simulations of Y segregation were performed with 0.1, 0.2, and 0.3 at.% Y in the present work. Results obtained in the present work will help understanding of segregation at a TJ and give clues for understanding origins of the enhanced ductility of Mg by Y addition.

II. METHODS

The {10$\bar{1}$1} and {10$\bar{1}$2} twin cell models are shown in figs. 1(a) and (b), respectively. Periodic boundary conditions were applied in the *x, y,* and *z* directions in the cells. The {10$\bar{1}$1}–{10$\bar{1}$2} DT cell model is shown in fig. 1(c), which is the same as the one used in a previous study.[26] Periodic boundary conditions were applied in the *x* direction in the cell. The cell model consisted of three regions (matrix, twin, and DT regions), {10$\bar{1}$1}, {10$\bar{1}$2}, and {30$\bar{3}$4} planes, and a TJ consisting of a {10$\bar{1}$1} and a {10$\bar{1}$2} TB. The {30$\bar{3}$4} plane is known to be the habit plane in Mg,[6,9] and it forms a component of the {10$\bar{1}$1}–{10$\bar{1}$2} DT.[19] The cell contained 21,944 atoms and the size of the cell was about $1.3 \times 21.8 \times 13.4$ nm^3 in the *x* (// [1$\bar{2}$10]), *y* (// [$\bar{1}$010]), and *z* (// [0002]) directions. The cell size was sufficient to calculate the segregation behavior in Mg DT.[26] The basal plane in the matrix region was parallel to the *x–y* plane of the simulation cell, the basal plane in the twin region was tilted at 56° with respect to the *x–y* plane, and the basal plane in the DT region was inclined at 38° with respect to the *x–y* plane. The basal plane in the twin region was tilted at 86° with respect to the
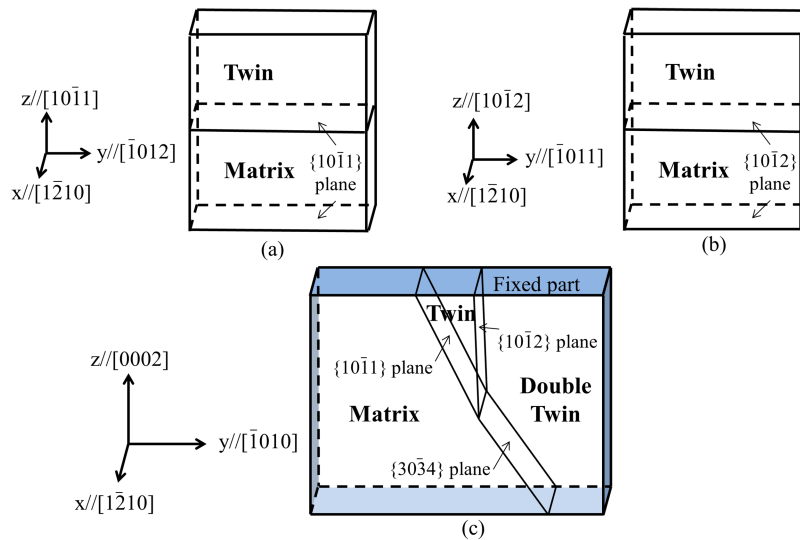

FIG. 1. Schematic illustrations of (a) {10$\bar{1}$1} TB, (b) {10$\bar{1}$2} TB, and (c) {10$\bar{1}$1}–{10$\bar{1}$2} DT cells in Mg. The DT consists of a {10$\bar{1}$1} TB, a {10$\bar{1}$2} TB, a TJ, and a {30$\bar{3}$4} boundary.

basal plane in the DT region. These orientations correspond to those in analytical[25] and experimental studies.[19,23,24,32,33] The distance from the left side of the cell to the TJ was 14.7 nm.

All of the simulations were performed using the AMEAM potential[34] in the NVT ensemble. The segregation energy at 2.5at%Y in Mg-Y system by using the AMEAM potential was -0.8 eV in the previous paper,[29] which almost agrees with the value (= -0.4 eV) by the first-principles calculation.[35] Molecular dynamics (MD) simulations were performed for 5 ps to relax the cell models. The temperature was fixed by the Nose–Hoover thermostat technique.[36] The MD time step was 1 fs. The cells were sufficiently relaxed at 5 K without applied stresses and strains. The boundary and TJ regions were defined as the region within 0.6 nm of the boundary plane[37–39] (i.e., the boundary width was 1.2 nm) and the region within 2 nm from the TJ point, respectively.

Segregation sites for Y atoms in the cells were examined by MC simulations. In the MC simulations, two types of events were repeated: small random displacements of randomly chosen Mg atoms (10% of the Mg atoms), and exchange of the atom identities between randomly chosen Mg and Y atoms.[40] The former event corresponds to thermal vibration and the latter event corresponds to placement of Y atoms into their equilibrium positions. The Metropolis algorithm was used to decide acceptance or rejection of a given movement. In the algorithm, the acceptance ratio is set as

$$W = 1 \qquad\qquad \text{if } \Delta E \leq 0$$
$$W = \exp(-\Delta E/kT) \quad \text{if } \Delta E > 0 \tag{1}$$

where W is the acceptance ratio, ΔE is the potential energy change, k is Boltzmann's constant, and T is the temperature of the system (5 K). The potential energy was calculated with the AMEAM potential used in the MD simulations. The maximum values of the small random displacements were adjusted so that the acceptance ratio was about 0.4. The two events were repeated for 50×21944 steps (50 MC steps). After the MC simulations, 10 ps MD simulations were performed to calculate the segregation energy. The segregation energy is given by[41]

$$E_{\text{Seg}} = \{[E_{\text{Boundary}}(\text{Mg}_{N-m}\text{Y}_m) - E_{\text{Boundary}}(\text{Mg}_N)] - m[E_{\text{Matrix}}(\text{Mg}_{M-1}\text{Y}) - E_{\text{Matrix}}(\text{Mg}_M)]\}/m \tag{2}$$

where $E_{\text{Boundary}}(\text{Mg}_{N-m}\text{Y}_m)$ is the total energy of a supercell containing boundaries, N is the number of atoms in the DT cell model, M is the number of Mg atoms, m is the number of Y atoms, $E_{\text{Boundary}}(\text{Mg}_N)$ is the total energy of a pure Mg supercell containing DT boundaries, $E_{\text{Matrix}}(\text{Mg}_{M-1}\text{Y})$ is the total energy of a twin-boundary-free supercell with $M-1$ Mg atoms and one Y atom, and $E_{\text{Matrix}}(\text{Mg}_M)$ is the total energy of a pure and perfect Mg supercell with M Mg atoms. The segregation energy was normalized by the number of segregated atoms. In the present work, N and M were 21944 and 21844, and m was 11 for the $\{10\bar{1}1\}$ twin, 13 for the $\{10\bar{1}2\}$ twin, 28 for the $\{30\bar{3}4\}$ boundary, and 14 for the TJ. Also, the volume and anisotropic factor of the atomic Voronoi polyhedron for each atom were calculated to investigate the geometric relations of atoms with the segregation behavior. The anisotropic factor at the segregated site was calculated by

$$f_{\text{anisotropic}} = \sqrt{\frac{1}{n}\sum(x_i - x_0)^2} \tag{3}$$

where $f_{\text{anisotropic}}$ is the anisotropic factor of the atomic Voronoi polyhedron at the segregated site, x_i is the distance between a segregated atom and its nearest neighbor atoms, x_0 is the average value of x_i, and n is the number of the nearest neighbor atoms. The nearest neighbor atoms were defined by the method reported by Honeycutt *et al.*,[42] where the minimum value of the pair correlation function is set as the nearest neighbor distance. The pair correlation function is given by

$$g(r) = \text{average}[g_i(r)] = \text{average}[n(r)]/4\pi r^2 dr\rho \tag{4}$$

where $g(r)$ is the pair correlation function, $n(r)$ is the number of atoms located from radius r to $r+dr$ from atom i, and ρ is the number density of atoms of the DT cell model. In the present study, $dr = 0.02$ Å.

III. RESULTS

Illustrations of Y segregation at a $\{10\bar{1}1\}$ TB and a $\{10\bar{1}2\}$ TB for 0.1 at.% Y are shown in fig. 2. Y atoms tended to be periodically located at the TB for both the $\{10\bar{1}1\}$ and $\{10\bar{1}2\}$ twins. The solute
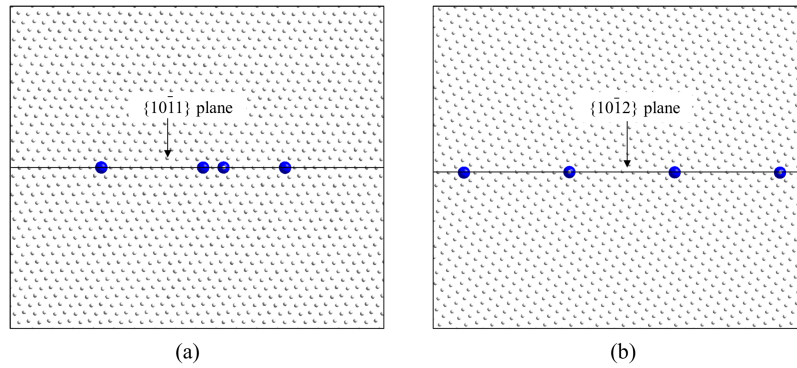
FIG. 2. Illustrations of Y segregation at a TB for 0.1 at.% Y: (a) a {10$\bar{1}$1} TB and (b) a {10$\bar{1}$2} TB. Blue spheres indicate yttrium atoms. Y atoms tended to be periodically located at the TB for both the {10$\bar{1}$1} and {10$\bar{1}$2} twins.

elements with large volumes tends to placed at the extension sites at TB to relax the extension strain. The atomic size of Y is larger than that of Mg, which is why Y atoms tended to be periodically located at the TBs.[41] The extension sites are the sites with large voronoi volumes.[41] Similar Y segregation behavior at the TBs was obtained for 0.2 at.% Y, although the number of segregated Y atoms was larger for 0.2 at.% Y than for 0.1 at.% Y.

Fig. 3 shows illustrations of Y segregation at the DT, and fig. 4 shows the density per cubic volume of Y atoms segregated at the DT. Y atoms segregated at the boundaries of the DT as well as the TBs. As shown in fig. 4, the density of Y atoms segregated at the TJ was as low as those at the TBs for 0.1 at.% Y, and it was lower than those at the other boundaries for 0.2 at.% Y. Purohit *et al.*[43] showed that solute atoms in Al–Pb alloys were more segregated at the TJ than at grain boundaries because the grain boundary energy decreased more by segregation at the TJ. However, the results of the present work suggest that the TJ is not always suitable for segregation. In addition, Y atoms were
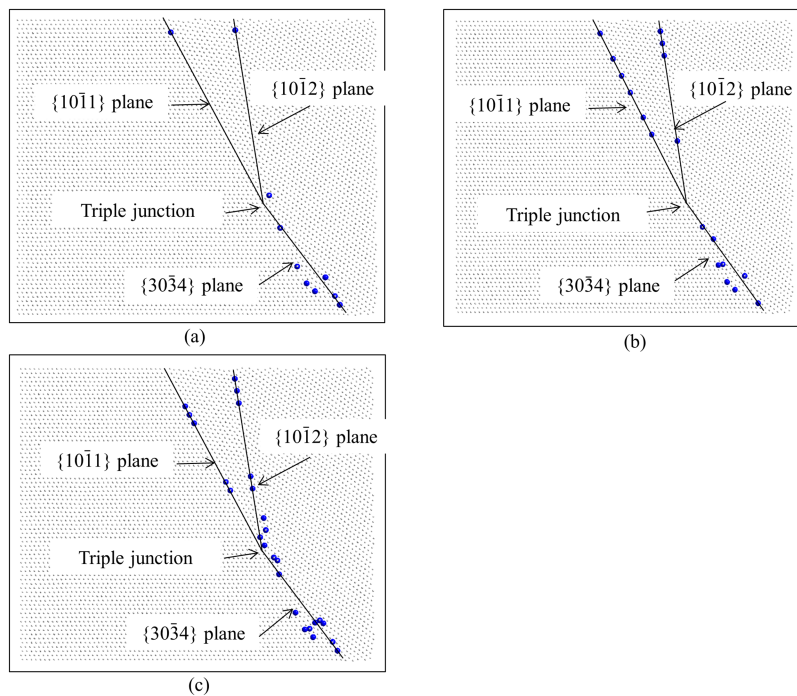

FIG. 3. Illustrations of Y segregation at the DT: (a) 0.1 at.% Y, (b) 0.2 at.% Y, and (c) 0.3 at.% Y. Blue spheres indicate yttrium atoms. Y atoms segregated at the DT as well as the TBs.
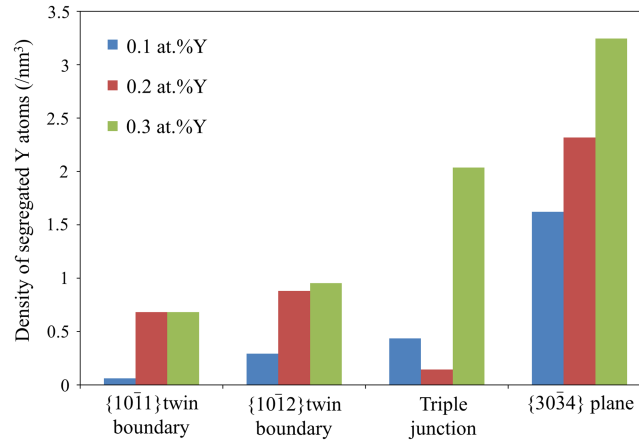
FIG. 4. Density per cubic volume of Y atoms segregated at the DT for 0.1, 0.2, and 0.3 at.% Y. The density of Y atoms segregated at the TJ was as low as those at the TBs for 0.1 at.% Y, and it was lower than those at the other boundaries for 0.2 at.% Y.

much more segregated at the TJ for 0.3 at.% Y than for 0.1 and 0.2 at.% Y. Thus, the Y segregation behavior at the TJ strongly depended on its concentration.

Schematic illustrations of the Voronoi volume at the $\{10\bar{1}1\}$ and $\{10\bar{1}2\}$ TBs are shown in fig. 5. Extension sites were periodically located at the TBs for both the $\{10\bar{1}1\}$ and $\{10\bar{1}2\}$ twins. These correspond to Y atoms periodically located at the TBs. Thus, the segregation behavior at the TBs can be understood from the viewpoint of the free volume.[41]

Fig. 6 shows a schematic illustration of the Voronoi volumes at the DT, and fig. 7 shows the average value of the Voronoi volume at extension sites of the DT. The free volumes at the extension sites of the TJ were larger on average than those of the other boundaries. However, Y atoms were not necessarily more segregated at the TJ than at the other boundaries, in particular, for 0.2 at.% Y. Clearly, the segregation behavior at the TJ cannot be explained only from the viewpoint of the free volume.

Fig. 8 shows the segregation energy at the DT for 0.3 at.% Y. The negative segregation energy indicates favorable segregation. The segregation energy at the TJ was almost the same as those at the other boundaries. The segregation energy was examined in the situation where many Y atoms were segregated, and the segregation energy of each Y atom depended on the site at the TJ. Thus, the complicated segregation behavior at the TJ cannot be understood from the segregation energy.
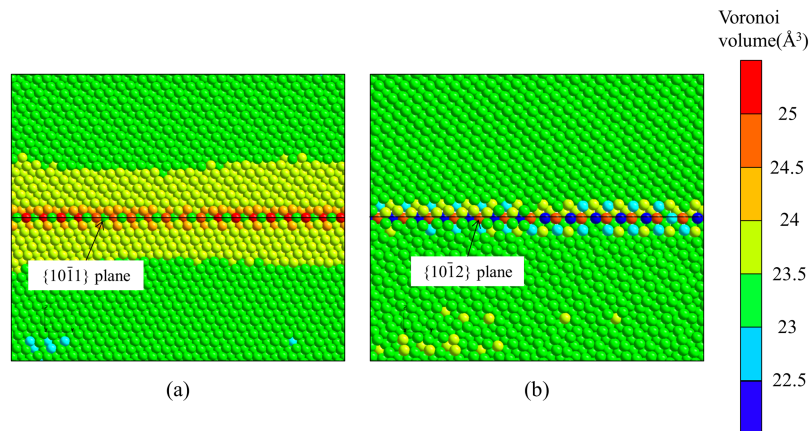

FIG. 5. Schematic illustrations of the Voronoi volume at a TB: (a) a $\{10\bar{1}1\}$ TB and (b) a $\{10\bar{1}2\}$ TB. Extension sites were periodically located at the TBs for both the $\{10\bar{1}1\}$ and $\{10\bar{1}2\}$ twins.
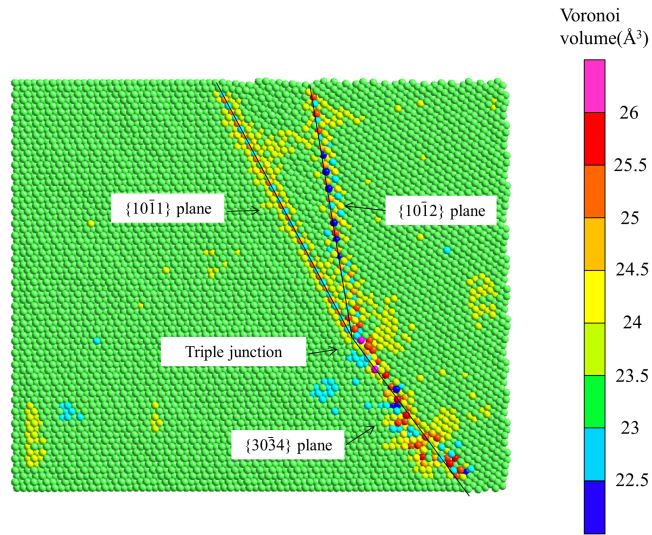
FIG. 6. Schematic illustration of the Voronoi volumes at the DT. The Voronoi volumes at the extension sites of the TJ are larger on average than those of the other boundaries.
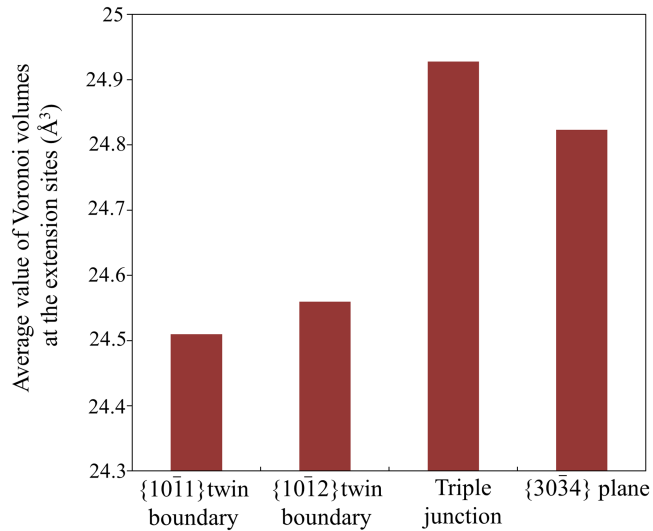

FIG. 7. Average values of the Voronoi volume at the extension sites of the DT. Y atoms were not necessarily more segregated at the TJ than at the other boundaries, in particular, for 0.2 at.% Y.

IV. DISCUSSION

There have been many atomistic simulation studies of grain boundary segregation.[37–39,43–53] Many studies[37,38,44,47–49] pointed out the importance of the size effect on grain boundary segregation, namely, the difference in atomic size between the segregation atom and the host atom was critical for grain boundary segregation. Huber *et al.*[49] investigated the binding energies of many alloying elements, such as Y and Al, to a Σ7 grain boundary in Mg. They noted that the binding energy scaled with the size of the solute and the local grain boundary site volume. However, the segregation energy depends not only on the size effect, but also on the excess cohesion energy effect.[37,44,47] When the bonding between a segregated atom and a host atom has strong ionic and/or covalent characteristics, the excess cohesion energy effect is likely to be critical for grain boundary segregation. The difference in the electronegativity of Y (1.22) and Mg (1.31) is not large. In addition, Mg–Y atomic bonding
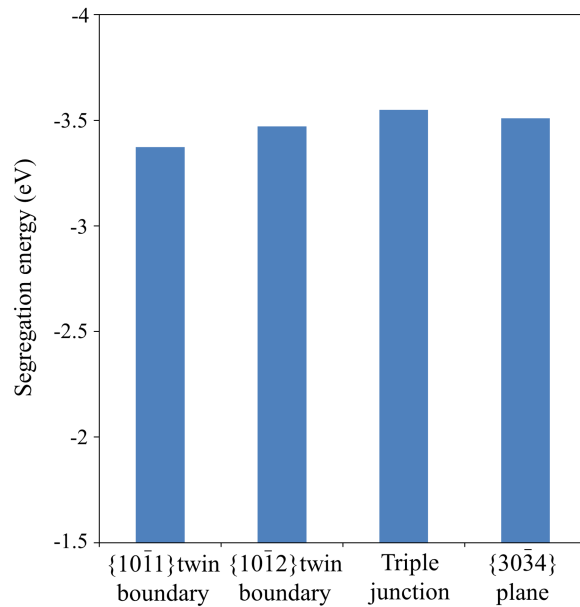
FIG. 8. Segregation energy of Y at the DT for 0.3 at.% Y. A negative segregation energy indicates favorable segregation. The segregation energy at the TJ was almost the same as those at the other boundaries.

seems to have no covalent characteristics.[54] Concerning the size effect, a segregation atom that is larger than the host atom is more effective for decreasing the grain boundary energy.[38] Hence, the size effect is likely to be predominant in Y segregation at Mg boundaries. In this situation, the Y segregation behavior at $\{10\bar{1}1\}$ and $\{10\bar{1}2\}$ TBs can be understood from the viewpoint of the free
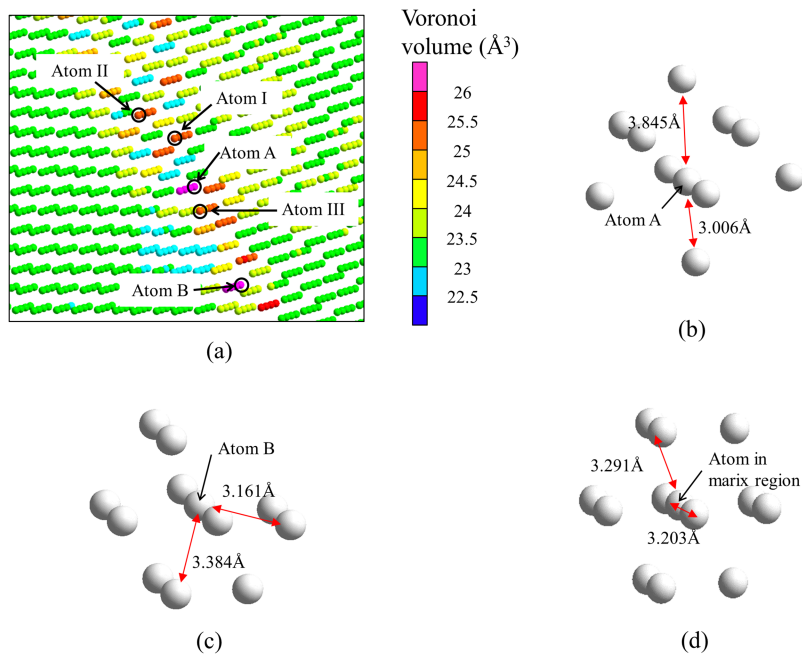
FIG. 9. (a) Microstructure of the TJ, (b) atomic configuration around atom A, (c) atomic configuration around atom B, and (d) atomic configuration around a host atom far away from the DT. The atom B site rather than the atom A site is the site for Y segregation. The atoms I, II, and III in (a) are used in Table I. The interatomic distances between the nearest neighbor atoms are almost the same for the host atom. However, they are different from one another for atoms A and B located at the TJ.

volume. However, the present work showed that the free volume is not the only determinant for Y segregation at the TJ even when the size effect is predominant for segregation.

Fig. 9(a) shows the microstructure of the TJ, (b) and (c) show the atomic configurations around atoms A and B shown in (a), and (d) shows the atomic configuration around a host atom far away from the DT, where the atom B site rather than the atom A site is the site for Y segregation. The interatomic distances between the nearest neighbor atoms are almost the same for the host atom. However, they are different from one another for atoms A and B located at the TJ. The volume and anisotropic factor of the atomic Voronoi polyhedron are 27.1 Å^3 and 0.255 for atom A, 26.2 Å^3 and 0.0653 for atom B, and 23.2 Å^3 and 0.0062 for the matrix atom, respectively. Thus, the anisotropic shape of the atomic Voronoi polyhedron is likely to be responsible for there being no Y segregation at the atom A site because of the large anisotropic factor of atom A. Therefore, it is suggested that not only the volume of the atomic Voronoi polyhedron, but also its shape affect the segregation behavior.

Fig. 10 shows the influence of the volume and anisotropic factor of the atomic Voronoi polyhedron on Y segregation at the DT, where the volume and anisotropic factor were calculated from the atomic configuration without Y segregation. From figs. 10(a) and (b), the Voronoi volume and anisotropic factor should be more than 24.2 Å^3 and less than 0.22 for Y segregation, although Y atoms are not segregated at all of the sites with a Voronoi volume more than 24.2 Å^3 and an anisotropic factor less than 0.22, which is partly because all of the sites at the boundaries were not investigated by the MC simulations.

Although the volume and the anisotropy of the atomic Voronoi polyhedron are important factors for Y segregation, all of the Y segregation events cannot be explained with only these two factors. Hence, there seem to be other factors that affect Y segregation. Table I lists the Voronoi volume, anisotropic factor, shortest interatomic distance between nearest neighbor atoms, and coordination
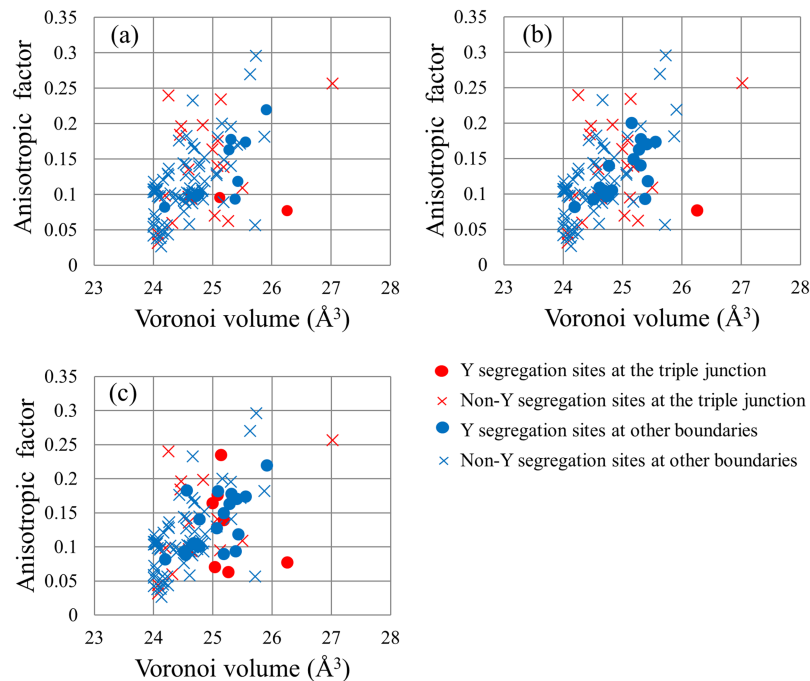

FIG. 10. Influence of the volume and anisotropic factor of the atomic Voronoi polyhedron on Y segregation at the DT: (a) 0.1 at.% Y, (b) 0.2 at.% Y, and (c) 0.3 at.% Y. The volume and anisotropic factor were calculated from the atomic configuration without Y segregation. The red circular mark indicates the site of the TJ where a Y atom is segregated, the red X mark indicates the site of the TJ where a Y atom is not segregated, the blue circular mark indicates the site of boundaries except for the TJ where a Y atom is segregated, and the blue X mark indicates the site of boundaries except for the TJ where a Y atom is not segregated. the Voronoi volume and anisotropic factor should be more than 24.2 Å^3 and less than 0.22 for Y segregation, although Y atoms are not segregated at all of the sites with a Voronoi volume more than 24.2 Å^3 and an anisotropic factor less than 0.22, which is partly because all of the sites at the boundaries were not investigated by the MC simulations.

TABLE I. Voronoi volume, anisotropic factor, shortest interatomic distance between nearest neighbor atoms, and coordination number of three atoms (I, II, and III, as shown in fig. 9(a)) located at the TJ. Atom I is the segregation site, and atoms II and III are not segregation sites for 0.1 at.% Y.

Atom site	Voronoi volume (Å^3)	Anisotropic factor	Shortest interatomic distance (Å)	Coordination number
I	25.12	0.095	3.138	12
II	25.18	0.139	3.089	12
III	25.04	0.070	3.135	11

number for three atoms I, II, and III, which are shown in fig. 9(a), located at the TJ. Atom I is the segregation site and atoms II and III are not segregation sites for 0.1 at.% Y. Comparing atom I with atom II, the difference in the shortest interatomic distance is large, while there are small differences in the other parameters. Comparing atom I with atom III, the coordination number of atom III is less than that of atom I. Thus, Y segregation at the TJ depends on the shortest interatomic distance and coordination number when the Voronoi volume and the anisotropic factor are almost the same. Hence, the main determinants for Y segregation may be the volume and anisotropic factor of the atomic Voronoi polyhedron, and the shortest interatomic distance and coordination number may secondarily affect Y segregation. Ziebarth *et al.*[53] performed a first-principles study of Fe segregation at Si grain boundaries. They noted that the segregation energy depended on the coordination number but the relation was not obvious between the segregation energy and the coordination number. Although it is difficult to develop quantitative relations between the determinants for grain boundary segregation, the present study can suggest qualitative descriptions of the determinants for enhanced Y segregation at Mg boundaries: an increase in the free volume, a decrease in the anisotropic factor of the atomic Voronoi polyhedron, an increase in the shortest interatomic distance, and an increase in the coordination number.

Another important result in the present work is that Y segregation at the TJ strongly depended on the Y concentration. The concentration dependence of segregation may be related to covalent interactions between segregated atoms.[45] Fig. 11 shows schematic illustrations of the atomic configuration at the DT for 0.3 at.% Y. For the $\{10\bar{1}1\}$ and $\{10\bar{1}2\}$ TBs, the distances between the segregated Y atoms are almost the same because of the periodic segregation of Y atoms. For the TJ, however, the distances are different, and the shortest distance between Y atoms is 3.3 Å. In the case of the short distance, strong covalent interactions may be generated between Y atoms, which will be discussed
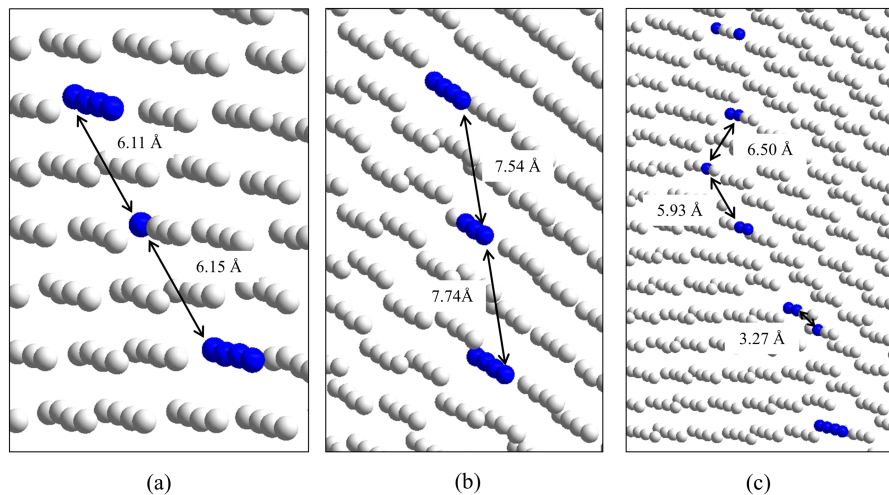

FIG. 11. Schematic illustrations of the atomic configurations at the DT for 0.3 at.% Y: (a) the $\{10\bar{1}1\}$ TB, (b) the $\{10\bar{1}2\}$ TB, and (c) the TJ. Blue sphere indicate segregated Y atoms. For the $\{10\bar{1}1\}$ and $\{10\bar{1}2\}$ TBs, the distances between the segregated Y atoms are almost the same because of the periodic segregation of Y atoms. For the TJ, however, the distances are different, and the shortest distance between Y atoms is 3.3 Å.
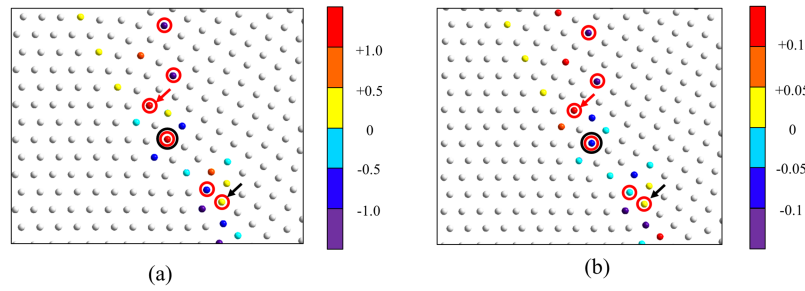
FIG. 12. Variation in the (a) volume and (b) anisotropic factor of Voronoi polyhedrons of atoms around the segregation site. The black circle indicates the segregation site where a Y atom is segregated for the first time, and the red circle indicates the sites where Y atoms are segregated for 0.3 at.% Y. Y atoms tend to segregate at sites where the anisotropic factor decreases, except for the two cases shown by the red and black arrows. Y atoms tended to segregate at sites where the anisotropic factor decreased, except for the two cases indicated by the red arrow and black arrow in fig. 12. At the site indicated by the red arrow, the free volume significantly increased. At the site indicated by the black arrow, both the free volume and anisotropic factor slightly increased.

later. However, in most cases, the Y–Y interatomic distances are large at the TJ as well as at the TBs. Therefore, it is suggested that covalent interactions between Y atoms only have a minor effect on Y segregation, and the concentration dependence of Y segregation at the TJ is mainly related to the size effect.

From fig. 10(c), for 0.3 at.% Y, Y atoms segregate at the TJ even when the anisotropic factor is larger than 0.22. The microstructure of the grain boundary can change with grain boundary segregation,[46] resulting in enhanced segregation.[39,55] Therefore, the atomic Voronoi polyhedrons around the segregation site may change when a Y atom is segregated at the TJ. Fig. 12 shows the variation of the volume and anisotropic factor of Voronoi polyhedrons of atoms around the segregation site. In fig. 12, the black circle indicates the site where a Y atom is segregated for 0.1at.% Y., and the red circle indicates the site where a Y atom is segregated for 0.3 at.% Y. Y atoms tended to segregate at sites where the anisotropic factor decreased, except for the two cases indicated by the red arrow and black arrow in fig. 12. At the site indicated by the red arrow, the free volume significantly increased. Therefore, it is suggested that the concentration dependence of Y segregation at the TJ is because of variation in the local atomic configuration with Y segregation, particularly the decrease in the anisotropic factor. At the site indicated by the black arrow, both the free volume and anisotropic factor slightly increased. In this case, the distance between Y atoms is very short. Hence, Y segregation at the site indicated by the black arrow may be related to covalent interactions between Y atoms. It can be expected that Y segregation disturbs subsequent Y segregation because the adjacent oversized Y atoms repel each other.[49] However, the present work suggests that variation in local atomic configuration decreases the anisotropic factor, resulting in enhanced Y segregation.

V. CONCLUSIONS

Monte Carlo simulations of Y segregation at a $\{10\bar{1}1\}$–$\{10\bar{1}2\}$ DT in Mg were performed with 0.1, 0.2, and 0.3 at.% Y, where the DT was composed of a $\{10\bar{1}1\}$ TB, a $\{10\bar{1}2\}$ TB, a $\{30\bar{3}4\}$ boundary, and a TJ. Y atoms segregated at the extension sites in the TBs. The Y segregation behavior at the TBs could be explained by the free volume. On the other hand, Y atoms were not necessarily more segregated at the extension sites in the TJ, although the free volumes were larger on average at the TJ than at the TBs. Not only the free volume, but also the anisotropic factor of atomic Voronoi polyhedrons determined Y segregation at the TJ. The shortest interatomic distance between nearest neighbor atoms and the coordination number also affected segregation. Another important result in the present work is that segregation at the TJ strongly depended on the Y concentration. The local atomic configuration changed around the segregation site. In particular, the anisotropic factor decreased, which resulted in a large Y concentration dependence of segregation at the TJ. Thus, the segregation behavior at the TJ was complicated, contrary to those at TBs, even when the size effect was predominant.

ACKNOWLEDGMENTS

[1] M. Všianská and M. Šob, Prog. Mater. Sci. **56**, 817 (2011).
[2] S. V. Divinski and H. Edelhoff, Phys. Rev. B **85**, 144104 (2012).
[3] Z. Pan and T. J. Rupert, Phys. Rev. B **93**, 134113 (2016).
[4] M. H. Yoo, Metall. Trans. A **12**, 409 (1981).
[5] J. Koike, Metall. Mater. Trans. A **36**, 1689 (2000).
[6] R. E. Reed-Hill and W. D. Robertson, Acta Metall. **5**, 717 (1957).
[7] R. E. Reed-Hill and W. D. Robertson, Acta Metall. **5**, 728 (1957).
[8] E. W. Kelley and W. F. Hosford, Jr., Trans. Metall. Soc. AIME **242**, 654 (1968).
[9] H. Yoshinaga, T. Obara, and S. Morozumi, Mater. Sci. Eng. **12**, 255 (1973).
[10] M. R. Barnett, Mater. Sci. Eng. A **464**, 1 (2007).
[11] M. R. Barnett, Mater. Sci. Eng. A **464**, 8 (2007).
[12] K. N. Braszczyńska-Malik, L. Lityńska, and W. Baliga, J. Microscope **224**, 15 (2006).
[13] M. R. Barnett, Z. Keshavarz, A. G. Beer, and D. Atwell, Acta Mater. **52**, 5093 (2004).
[14] A. Serra and D. J. Bacon, Acta Metall. Mater. **43**, 4465 (1995).
[15] M. Yuasa, K. Masunaga, M. Mabuchi, and Y. Chino, Phil. Mag. **94**, 285 (2014).
[16] B. C. Wonsiewicz and W. A. Backofen, Trans. Metall. Soc. AIME **239**, 1422 (1967).
[17] S. Niknejad, S. Esmaeili, and N. Y. Zhou, Acta Mater. **102**, 1 (2016).
[18] A. Jain, O. Duygulu, D. W. Brown, C. N. Tomé, and S. R. Agnew, Mater. Sci. Eng. A **486**, 545 (2008).
[19] P. Cizek and M. R. Barnett, Scripta Mater. **59**, 959 (2008).
[20] D. Ando, J. Koike, and Y. Sutou, Acta Mater. **58**, 4316 (2010).
[21] J. Koike, N. Fujiyama, D. Ando, and Y. Sutou, Scripta Mater. **63**, 747 (2010).
[22] M. Lentz, R. S. Coelho, B. Camin, C. Fahrenson, N. Schaefer, S. Selve, T. Link, I. J. Beyerlein, and W. Reimers, Mater. Sci. Eng. A **610**, 54 (2014).
[23] É. Martin, L. Capolungo, L. Jiang, and J. J. Jonas, Acta Mater. **58**, 3970 (2010).
[24] M. R. Barnett, Z. Keshavarz, A. G. Beer, and X. Ma, Acta Mater. **56**, 5 (2008).
[25] I. J. Beyerlein, J. Wang, M. R. Barnett, and C. N. Tomé, Proc. R Soc. A **468** 1496 (2012).
[26] M. Yuasa, K. Masunaga, T. Yoshida, M. Mabuchi, and Y. Chino, Acta Mater. **61**, 4714 (2013).
[27] H. Somekawa, Y. Osawa, A. Singh, K. Washio, A. Kato, and T. Mukai, Mater. Trans. **55**, 182 (2014).
[28] Y. Chino, K. Sassa, and M. Mabuchi, Mater. Sci. Eng. A **513–514**, 394 (2009).
[29] T. Yoshida, M. Yuasa, M. Mabuchi, and Y. Chino, J. Appl. Phys. **118**, 034304 (2015).
[30] B. Q. Shi, R. S. Chen, and W. Ke, Mater. Sci. Eng. A **560**, 62 (2013).
[31] J. Chen, Z. Wang, X. Ma, X. Wang, Y. Lei, and W. Yan, J. Alloys Comp. **642**, 92 (2015).
[32] M. D. Nave and M. R. Barnett, Scripta Mater. **51**, 881 (2005).
[33] J. J. Jonas, S. Mu, T. Al-Samman, G. Gottstein, L. Jiang, and E. Martin, Acta Mater. **59**, 2046 (2011).
[34] W. Hu, B. Zhang, B. Huang, F. Gao, and D. J. Bacon, J. Phys. Condens. Mater. **13**, 1193 (2001).
[35] J. Zhang, Y. Dou, and Yi Zheng, Scr. Mater. **80**, 17 (2014).
[36] S. Melchionna, G. Ciccotti, and H. B. L. Hoover, Mol. Phys. **78**, 533 (1993).
[37] B. Lezzar, O. Khalfallah, A. Larere, V. Paidar, and O. Hardouin Duparc, Acta Mater. **52**, 2809 (2004).
[38] P. C. Millett, R. Panneer Selvam, S. Bansal, and A. Saxena, Acta Mater. **53**, 3671 (2005).
[39] J. A. Brown and Y. Mishin, Acta Mater. **53**, 2149 (2005).
[40] S. Jang, Y. Purohit, D. L. Irving, C. Padgett, D. Brenner, and R. O. Scattergood, Acta Mater. **56**, 4750 (2008).
[41] J. F. Nie, Y. M. Zhu, J. Z. Liu, and X. Y. Fang, Science **340**, 957 (2013).
[42] J. D. Honeycutt and H. C. Anderson, J. Phys. Chem. **91**, 4950 (1987).
[43] Y. Purohit, L. Sun, D. L. Irving, R. O. Scattergood, and D. W. Brenner, Mater. Sci. Eng. A **527**, 1769 (2010).
[44] F. Berthier, B. Legrand, and G. Tréglia, Acta Mater. **47**, 2705 (1999).
[45] D. I. Thomson, V. Heine, M. C. Payne, N. Marzari, and M. W. Finnis, Acta Mater. **48**, 3623 (2000).
[46] X. Xie and Y. Mishin, Acta Mater. **50**, 4303 (2002).
[47] O. H. Duparc, A. Larere, B. Lezzar, O. Khalfallah, and V. Paidar, J. Mater. Sci. **40**, 3169 (2005).
[48] Y. A. Du, L. Ismer, J. Rogal, T. Hickel, J. Neugebauer, and R. Drautz, Phys. Rev. B **84**, 144121 (2011).
[49] L. Huber, J. Rottler, and M. Militzer, Acta Mater. **80**, 194 (2014).
[50] S. K. Shattacharya, M. Kohyama, S. Tanaka, and I. Shiihara, J. Phys.: Condens. Matter. **26**, 355005 (2014).
[51] H. Wang, M. Kohyama, S. Tanaka, and Y. Shiihara, J. Mater. Sci. **50**, 6864 (2015).
[52] D. D. Stefano, M. Mrovec, and C. Elsässer, Acta Mater. **98**, 306 (2015).
[53] B. Ziebarth, M. Mrovec, C. Elsässer, and P. Gumbsch, Phys. Rev. B **91**, 035309 (2015).
[54] Q. Chen, Z. Huang, Z. Zhao, and C. Hu, Comput Mater. Sci. **67**, 196 (2013).
[55] M. Herbig, M. Kuzmina, C. Haase, R. K. W. Marceau, I. Gutierrez-Urrutia, D. Haley, D. A. Molodov, P. Choi, and D. Raabe, Acta Mater. **83**, 37 (2015).